Acta Poloniae Pharmaceutica – Drug Research, Vol. 69 No. 4 pp. 763–772, 2012 ISSN 0001-6837
Polish Pharmaceutical Society

## GENERAL

# 3D-QSAR STUDIES OF SOME TETRASUBSTITUTED PYRAZOLES AS COX-II INHIBITORS

GIRISH KUMAR GUPTA[1]* and AJAY KUMAR[2]

[1]M.M. College of Pharmacy, M.M. University, Mullana (Ambala), Haryana, India
[2]Institute of Pharmaceutical Science, Kurukshetra University, Kurukshetra, Haryana, India

**Abstract:** Pharmacophore mapping studies were undertaken for a series of molecules belonging to tetrasubstituted pyrazoles as canine COX-II inhibitors. A six point pharmacophore with 3 hydrogen bond acceptors (A), one hydrophobic group (H) and two aromatic rings (R) as pharmacophoric feature was developed. The pharmacophoric hypothesis yielded a statistically significant 3D-QSAR model, with a correlation coefficient of $r^2$ = 0.958. The developed pharmacophore model was externally validated by predicting the activity of test set molecules. The squared predictive correlation coefficient of 0.852 was observed between experimental and predicted activity values of test set molecules. The geometry and features of pharmacophore model describe the key structure-activity relationship of COX-II inhibitors, can predict their activities, and can thus be used to design novel inhibitors.

**Keywords:** COX-II inhibitors, PHASE, pharmacophore mapping, 3D-QSAR

The non-steroidal anti-inflammatory drugs (NSAIDs) are the widely useful therapeutic agents useful in the treatment of various inflammatory diseases. However, long term use of those agents has been associated with various gastrointestinal (GI) toxicities (1, 2) The prostaglandin (PG) synthase (cyclooxygenase), the key enzyme of inflammatory process, and an important target of most of the currently used NSAIDs, exists in main two isoforms (COX-I and COX-II) (3, 4). COX-I is constitutively expressed and is responsible for several physiological functions, whereas COX-II is an inducible isoenzyme involved in the inflammation (5). Inhibition of COX-I by conventional NSAIDs produced toxicity and adverse effects, in particular GI ulcers and renal failure (6). The beneficial anti-inflammatory and analgesic activities are based in the inhibition of COX-II, but the gastrointestinal toxicity and other side effects are due to the concurrent inhibition of COX-I (7). Agents which inhibit COX-II, while sparing COX-I, represent a new therapeutics goal for development of safer NSAIDs (8–12). However, the selective COX-II inhibitors, viz., nimesulide, celecoxib, rofecoxib, valdecoxib and etoricoxib treat the chronic rheumatoid and osteoarthritis without causing GI damage (13–17). A few COX-II inhibitors have also been studied for the treatment of cancer and Alzheimer's disease (18, 19). However, the recent withdrawal of rofecoxib from the market due to adverse cardiovascular side effects has raised the concern of safety of selective COX-II inhibitors (20). So, it is desirable to discover safe, potent, selective and patient-acceptable COX-II inhibitors to completely abandon the use of steroidal and narcotic drugs. Pyrazole is an important pharmacophore which exhibits widespread pharmacological properties such as analgesic, antipyretic, antiarthritic, antirheumatic and uricosuric activities (21).

Discovering three dimensional pharmacophores, which can explain the activity of a series of ligands, is one of the most significant contributions of computational chemistry to drug discovery (22). Quantitative drug design comprehends two major activities, the quantitative description of the structural differences among series of chemical compounds of biological interest, and the formulation of "QSAR" useful in the design of new and better therapeutic agents (23). QSAR is a mathematical relationship between a biological activity of a

* Corresponding author: e-mail: girish_pharmacist92@rediffmail.com; phone: 091-8059930169

molecular system and its geometric and chemical characteristics. QSAR attempts to find consistent relationship between biological activity and molecular properties, so that these "rules" can be used to evaluate the activity of new compounds. 3D models are more easily interpretable than 2D descriptor or fingerprint-based QSAR models, making it easier to suggest new compounds for synthesis. It should also be possible to make connections from such activity models to structure-based design, either to add more information to overlays for the construction of a pharmacophore model or to use a pharmacophore to assist in the refinement of protein homology models (24). In the present model, QSAR model has been developed for the prediction of COX-II inhibitory activity. 3D QSAR approach has been developed using PHASE module of Schrödinger suite (25).

## MATERIALS AND METHODS

All computations for the generation of pharmacophore models were performed with PHASE. We collected a series of COXIBs to generate pharmacophore models on the basis of their activity levels and structures. Twenty four COXIBs (1–24, Table 1) with a tetrasubstituted pyrazole skeleton were selected as the training set for pharmacophore models. Their activities ranged from (0.03 µM to 7.9 µM). Seven highly active COXIBs (25–31, Table 1) with various structures were used to formulate the pharmacophore hypotheses. Their structures and activities are shown in Table 1. All structures were built using a maestro and were minimized to a local energy minimum using the OPLS-2005 force field. Since molecules might adjust their conformations when binding to a receptor, conformational models consisting of a representative set of conformers were generated to increase their flexibility.

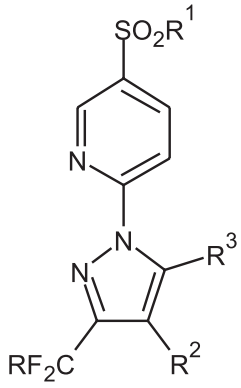


Figure 1. General structure of tetrasubstituted pyrazoles

### Biological data

For the pharmacophore modeling studies, a set of 31 COX-II inhibitory activity data ($IC_{50}$) was selected from the literature (26). The basic structure of all the data used is depicted in Figure 1 and various substituents are enlisted in Table 1. The data set was divided into training set and test set. The training set was selected randomly by considering the 75% of training set and 25% of test set. The training set consisted of 24 compounds selected and to validate our pharmacophore, the other 7 compounds were used as the test set.

### Preparation of ligands

The first step for the pharmacophore mapping was ligand preparation. The structures were imported from project table in the 'Develop Pharmacophore Hypothesis' panel and geometrically refined using ligprep (27). Ligprep attaches hydrogen, convert 2D structure to 3D, generates stereoisomers and optionally, neutralizes charged structure or determine the most probable ionization states at a user-defined pH. Tautomers were generated using Macro Model method discarding current conformers. The conformations were generated by the Monte-Carlo Multiple Minimum (MCMM)/low mode (LMOD) (28, 29) method using a maximum of 2,000 steps with a distance-dependent dielectric solvent model and an OPLS-2005 force field (30). All the conformers were subsequently minimized using truncated Newton conjugate gradient minimization up to 500 iterations. For each molecule, a set of conformers with a maximum energy difference 30 kcal/mol relative to the global energy minimum conformer were retained.

### Generation of common pharmacophore hypothesis (CPH)

The common pharmacophore hypothesis and alignment based on it was carried out using PHASE. Five pharmacophore features: hydrogen bond acceptor (A), hydrogen bond donor (D), hydrophobic group (H), negatively charged group (P) and aromatic ring (R) were defined by a set of chemical structure patterns as SMART (31) queries and aligned one of three possible geometrics that define the physical characteristics of the site:

1. Point – Site is located on a single atom in SMART query.

2. Vector – Site is located on a single atom in the SMART query and assigned directionality according to one or more vectors originating from the atom.

Table 1. Data set used in the generation of the pharmacophore for canine COX-II inhibitors.

| Training set | | | | | |
|---|---|---|---|---|---|
| Compound | R | $R^1$ | $R^2$ | $R^3$ | $IC_{50}$ (μM) |
| **1** | F | Me | CN | 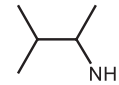 | 0.132 |
| **2** | F | Me | CN | 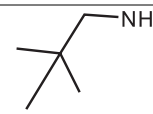 | 0.23 |
| **3** | F | Me | CN | 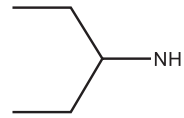 | 0.197 |
| **4** | F | Me | CN | 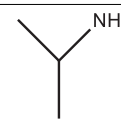 | 0.36 |
| **5** | F | Me | CN | 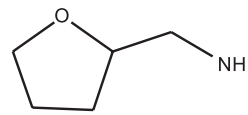 | 0.063 |
| **6** | F | Me | CN | 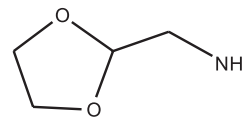 | 0.126 |
| **7** | F | Me | CN | 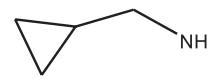 | 0.11 |
| **8** | F | Me | CN | 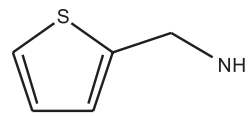 | 0.125 |
| **9** | F | Me | CN | 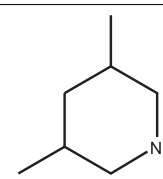 | 0.095 |
| **10** | F | Me | CN | 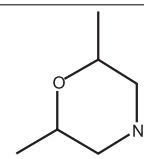 | 0.14 |
| **11** | F | Me | H | 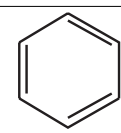 | 0.31 |
| **12** | H | Me | CN | 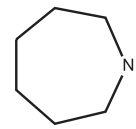 | 0.13 |
| **13** | H | Me | CN | 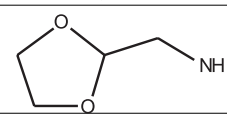 | 0.19 |

Table 1. cont

| | | | | | |
|---|---|---|---|---|---|
| **14** | H | Me | CN | 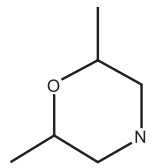 | 0.24 |
| **15** | H | Me | CN | 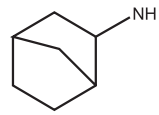 | 0.42 |
| **16** | F | $NH_2$ | CN | 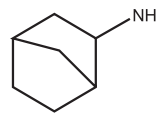 | 0.14 |
| **17** | F | $NH_2$ | CN | 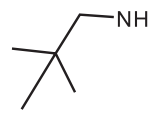 | 0.13 |
| **18** | F | $NH_2$ | CN | 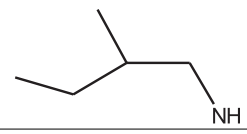 | 0.19 |
| **19** | F | $NH_2$ | CN | 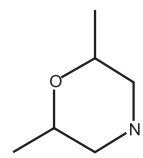 | 1.87 |
| **20** | F | $NH_2$ | CN | 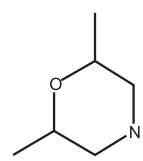 | 7.9 |
| **21** | H | $NH_2$ | CN | 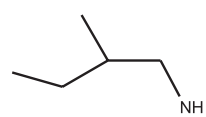 | 0.20 |
| **22** | H | $NH_2$ | CN | 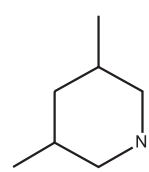 | 0.21 |
| **23** | H | $NH_2$ | CN | 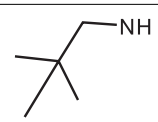 | 0.36 |
| **24** | H | $NH_2$ | CN | 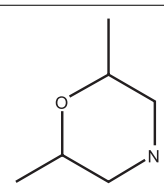 | 5.0. |

Table 1. cont

| Test set | | | | | |
|---|---|---|---|---|---|
| **25** | F | Me | CN | 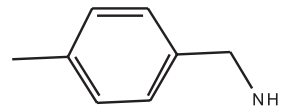 | 0.115 |
| **26** | F | Me | CN | 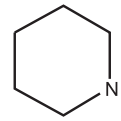 | 0.150 |
| **27** | F | Me | CN | 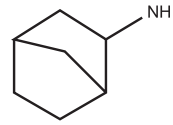 | 0.144 |
| **28** | F | Me | CN | 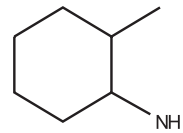 | 0.297 |
| **29** | H | Me | CN | 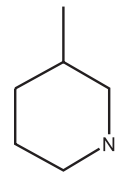 | 0.03 |
| **30** | H | Me | CN | 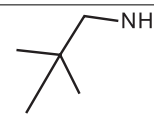 | 0.20 |
| **31** | F | NH2 | CN | 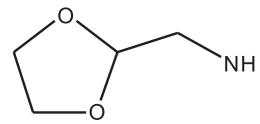 | 1.25 |

3. Group – Site is located at the centre of a group of atoms in the SMART query. For aromatic ring, the site is assigned directionality, defined by a vector that is normal to the plane of the ring.

Common pharmacophore feature were then identified from a set of variants – a set of feature type that define a possible pharmacophore – using a tree-based partitioning algorithm with maximum tree depth. The final size of the pharmacophore box was 1 Å, to optimize the number of final CPHs. The smaller is the box size the more closely pharmacophores must match. Any single pharmacophore in the group could ultimately become a common pharmacophore hypothesis. These analyses indicate that maximum sites can match only up to molecules out of 31. These CPHs were examined using a scoring function to yield the best alignment of active ligands, quality of alignment of active ligands and quality of alignment measured by a survival score, which defines as:

$$S = W_{site}\, S_{site} + W_{vec}\, S_{vec} + W_{vol}\, S_{vol} + W_{sel}\, S_{sel} + Wm_{rew}$$

where $W$ are weights and $S$ are scores; $S_{site}$ represents alignment score, the RMSD in the site point position; $S_{vec}$ represents vector score, and averages the cosine of the angles formed by corresponding pairs of vector features in aligned structures; $S_{vol}$ represents volume score based on overlap of van der Waals models of non hydrogen atoms in each pair of structures; and $S_{sel}$ represents selectivity score, and accounts for what fractions of molecules are likely to match the hypothesis regardless of their activity towards the receptor.

$W_{site}$, $W_{vec}$, $W_{vol}$, $W_{rew}$ have default values of 1.0, while $W_{sel}$ has a default value of 0.0. In hypothesis generation, default values have been used. $Wm_{rew}$ represents reward weights defined by m-1 where m

Table 2. Angles between different pharmacophoric sites of model AAAHR224.

| Site1 | Site2 | Site3 | Angle (deg.) | Site1 | Site2 | Site3 | Angle (deg.) | Site1 | Site2 | Site3 | Angle (deg.) |
|---|---|---|---|---|---|---|---|---|---|---|---|
| A4 | A1 | A5 | 13 | A1 | A5 | H6 | 21.3 | A1 | R9 | A5 | 148.8 |
| A4 | A1 | H6 | 56.5 | A1 | A5 | R9 | 10.1 | A1 | R9 | H6 | 72.7 |
| A4 | A1 | R9 | 12.1 | A1 | A5 | R10 | 16.7 | A1 | R9 | R10 | 152.5 |
| A4 | A1 | R10 | 4.4 | A4 | A5 | H6 | 72.1 | A4 | R9 | A5 | 19 |
| A5 | A1 | H6 | 65.5 | A4 | A5 | R9 | 78.6 | A4 | R9 | H6 | 124.2 |
| A5 | A1 | R9 | 21.2 | A4 | A5 | R10 | 70.5 | A4 | R9 | R10 | 11.6 |
| A5 | A1 | R10 | 8.7 | H6 | A5 | R9 | 11.6 | A5 | R9 | H6 | 137 |
| H6 | A1 | R9 | 44.9 | H6 | A5 | R10 | 13.5 | A5 | R9 | R10 | 9.1 |
| H6 | A1 | R10 | 59 | R9 | A5 | R10 | 9.1 | H6 | R9 | R10 | 134.8 |
| R9 | A1 | R10 | 14.1 | A1 | H6 | A4 | 103.1 | A1 | R10 | A4 | 167.2 |
| A1 | A4 | A5 | 79.8 | A1 | H6 | A5 | 93.2 | A1 | R10 | A5 | 154.6 |
| A1 | A4 | H6 | 20.4 | A1 | H6 | R9 | 62.4 | A1 | R10 | H6 | 32.9 |
| A1 | A4 | R9 | 5.9 | A1 | H6 | R10 | 88.2 | A1 | R10 | R9 | 13.5 |
| A1 | A4 | R10 | 8.4 | A4 | H6 | A5 | 14.5 | A4 | R10 | A5 | 38 |
| A5 | A4 | H6 | 93.4 | A4 | H6 | R9 | 40.9 | A4 | R10 | H6 | 138.5 |
| A5 | A4 | R9 | 82.4 | A4 | H6 | R10 | 15.5 | A4 | R10 | R9 | 156.7 |
| H6 | A4 | R9 | 14.8 | A5 | H6 | R9 | 31.4 | A5 | R10 | H6 | 158.2 |
| H6 | A4 | R10 | 26 | A5 | H6 | R10 | 8.2 | A5 | R10 | R9 | 161.9 |
| R9 | A4 | R10 | 11.7 | R9 | H6 | R10 | 25.8 | H6 | R10 | R9 | 19.4 |
| A1 | A5 | A4 | 87.1 | A1 | R9 | A4 | 162 | | | | |

Table 3. Distances between different pharmacophoric sites of model AAAHR224

| Site 1 | Site 2 | Distance (Å) | Site1 | Site 2 | Distance (Å) |
|---|---|---|---|---|---|
| A1 | A4 | 11.278 | A4 | R10 | 3.892 |
| A1 | A5 | 11.114 | A5 | H6 | 10.128 |
| A1 | H6 | 4.044 | A5 | R9 | 7.734 |
| A1 | R9 | 3.753 | A5 | R10 | 3.914 |
| A1 | R10 | 7.450 | H6 | R9 | 2.991 |
| A4 | A5 | 2.544 | H6 | R10 | 6.388 |
| A4 | H6 | 9.652 | H9 | R10 | 3.917 |
| A4 | R9 | 7.648 | | | |

Table 4. Experimental and predicted $IC_{50}$ values of test set molecules based on hypothesis AAAHR224.

| Comp. No | Experimental $IC_{50}$ (μM) | Predicted $IC_{50}$ (μM) | Residual activity |
|---|---|---|---|
| **25** | 0.115 | –1.08 | –1.195 |
| **26** | 0.150 | 0.06 | –0.090 |
| **27** | 0.144 | –1.0 | –1.144 |
| **28** | 0.297 | 0.79 | 0.493 |
| **29** | 0.03 | –0.023 | –0.053 |
| **30** | 0.2 | –0.84 | –1.04 |
| **31** | 1.25 | 3.24 | 1.99 |

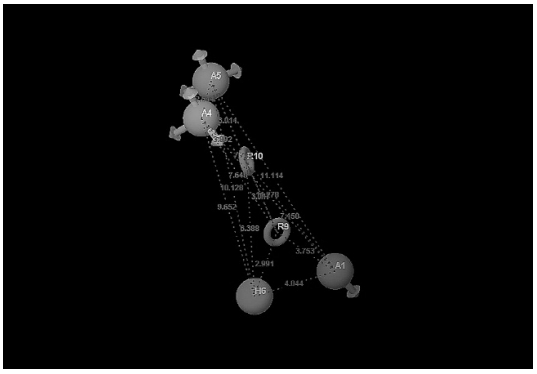


Figure 2. PHASE generated pharmacophore model AAAHR224 illustrating hydrogen bond acceptor (A1, A4, A5; spheres with pointed arms), aromatic ring (R9, R10; rings) and hydrophobic ring (H6; sphere without arms)

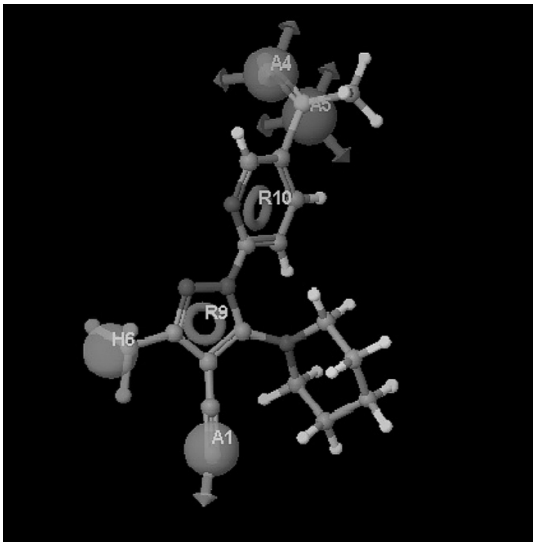


Figure 3. Best pharmacophore model AAAHR224 aligned with the most active compound **26** ($IC_{50}$ = 0.15 µM) of the test set. Pharmacophore features are coded: hydrogen bond acceptor (spheres with pointed arms), aromatic ring (rings) and hydrophobic ring (sphere without pointed arms)

is the number of actives that match the hypothesis (32).

**QSAR model building**

Phase provides the means to build the 3D QSAR model for a set of ligands that are aligned to a selected hypothesis. A training set of 24 molecules was selected randomly incorporating biological and chemical diversity and was used to generate atom-based QSAR models for all hypotheses using a grid spacing of 1Å. Models containing three partial least squares (PLS) factors tended to fit the $IC_{50}$ values beyond their experimental uncertainty. Each of these models was validated using an external set of 31 molecules that were not considered during model generation.

**Validation of generated pharmacophore**

The generated pharmacophore model should be statistically significant i.e., its regression coefficient should be good, its root mean standard error (RMSE) should be minimal, should predict activity of the new molecules accurately and should identify active compounds from the data base. Therefore, the derived pharmacophore map was validated using test for prediction.

**RESULTS AND DISCUSSION**

The cyclooxygenase enzymes (COX), which catalyze the first step in arachidonic acid metabolism, were identified as the molecular targets of all NSAIDs. The purpose of pharmacophore modeling is to perform *in silico* screening searches in a 3 dimensional data base of a virtual or real compound to find diverse structure with desired activity and lower side effects. In the present studies, a series of tetrasubstituted pyrazoles were considered for molecular modeling studies. The studies were aimed at developing a ligand based pharmacophore model relating the canine COX II-ligand interaction.

Twenty four molecules forming the training set were used to develop the pharmacophore. The pharmacophoric feature selected for creating sites were hydrogen bond acceptor (A), hydrophobic region (H), and aromatic ring (R). Pharmacophore models containing six sites, i.e., features were generated. Six featured pharmacophore hypotheses were selected and subjected to stringent scoring function analysis.

The results of six featured pharmacophore hypotheses are labeled as AAAHR224, AAAHR1265, AAAHRR229, AAAHRR206, AAAHRR226, AAAHRR221, AAAAHR221, AAAAHR1279, AAAHR210, AAAHR217, AAAHRR233, AAAHRR214, AAAAHR1256, AAAHRR230, AAAAHR280, AAAAHR1293, AAAAHR1276, AAAAHR1275, AAAAHR1264, AAAAHR1353 and AAAAHR1302. The first hypothesis AAAHR224 is the best hypothesis in this study, characterized by highest survival score, highest F value and the best regression coefficient (0.958). The AAAHR224 pharmacophore hypothesis is presented in Figure 2. The features represented by this hypothesis are three hydrogen bond acceptors (A), one hydrophobic region (H), and two aromatic rings (R). The angles and distances

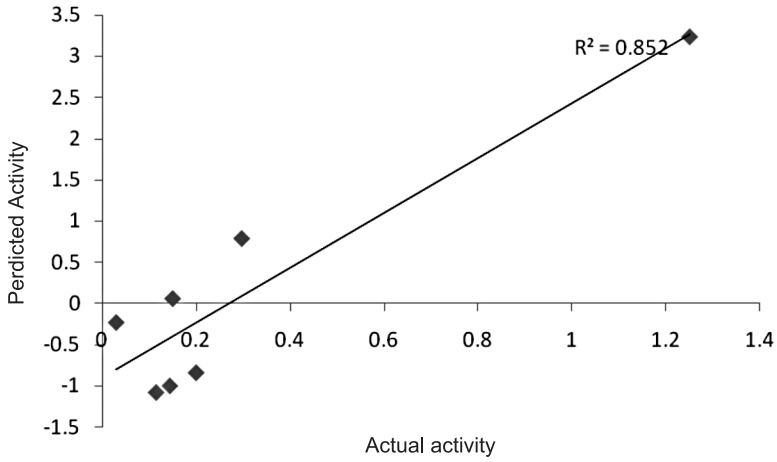


Figure 4. Relation between experimental and predicted COX-II inhibitory activity values of test set molecules using model AAAHR224

between different sites of AAAHR224 are given in Table 2 and 3, respectively.

For each ligand, one aligned conformer based on the lowest RMSE of feature atom coordinates from those of the corresponding reference feature was superimposed on hypothesis. Then, fitness scores for all ligands were observed on the best scored pharmacophore model. The greater the fitness score, the greater the activity prediction of the compound. The fit function does not only check if feature is mapped or not, it also contains a distance term, which measures the distance that separates the feature on the molecule from the centroid of the hypothesis feature. Figure 3 shows the AAAHR224 aligned with the most active compound 12 ($IC_{50}$ = 0.15 μM) of the test set.

Besides this survival score analysis, the validity and predictive character of AAAHR224 were further assessed by predicting the activity of test set molecules. A test set having seven molecules was analyzed. All the test set molecules were built and minimized as well as used in conformational analysis like all training set molecules. Then, the activities of test set molecules were predicted using AAAHR224 and compared with the actual activity. Actual and predicted activity values of test set molecules are given in Table 4. The predicted COX-II inhibitory activity exhibited a correlation of 0.852 with reported COX-II inhibitory activity using model AAAHR224 (Fig. 4). For a reliable model, the squared predictive correlation coefficient should be > 0.60. The results of this study reveal that model AAAHR224 can be used for the prediction of COX-2 inhibitory activity. Good and consistent external predictivity was observed for AAAHR224 as compared to the other hypotheses. AAAHR224 showed a good $r^2$ value, i.e., 0.958 and squared predictive correlation coefficient of 0.852 was also observed between experimental and predicted activity values of test set molecules.

**Interpretation of QSAR model**

Additional insight into the inhibitory activity can be gained by visualizing the QSAR model in the context of one or more ligands in the series with varying activity. This information can then be used to design new and more active analogues. A pictorial representation of the contours generated is shown in Figure 5a–d. In these representations, the blue cubes (denoted by cubes filled with vertical lines) indicate favorable regions while red cubes (denoted by cubes filled with square boxes) indicate unfavorable regions for activity.

Figure 5a and 5b compare the QSAR model in the context of the hydrogen bond donor property for the more active molecule 16 and the less active molecule 27. The blue region was observed near the 5-methyl substituted sulfonyl-pyridin-2-yl-1*H*-pyrazole, thus, molecules with a potential hydrogen bond donor at this position showed high activity. Red region observed near the 5-aryl position of the pyrazole and hydrogen bond donor substitution at this position lower the activity.

Figure 5c illustrates the significant favorable and unfavorable hydrophobic interactions, which arise when the QSAR model is applied to the most active molecule **16**. Big red region denoted by cubes

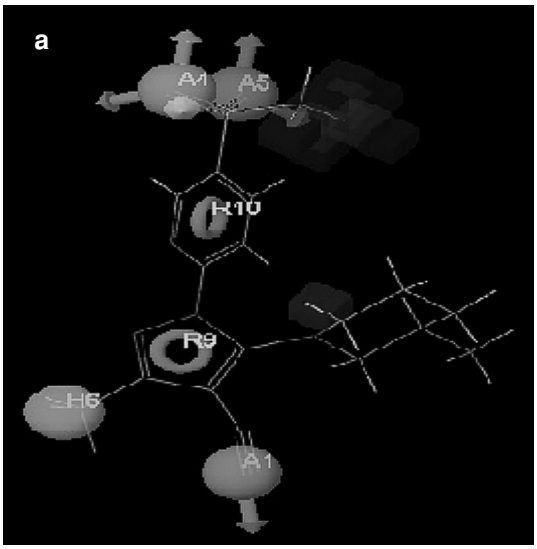


Figure 5a. 3-D QSAR model based on more active compound **16** of the training set illustrating hydrogen bond donor feature.

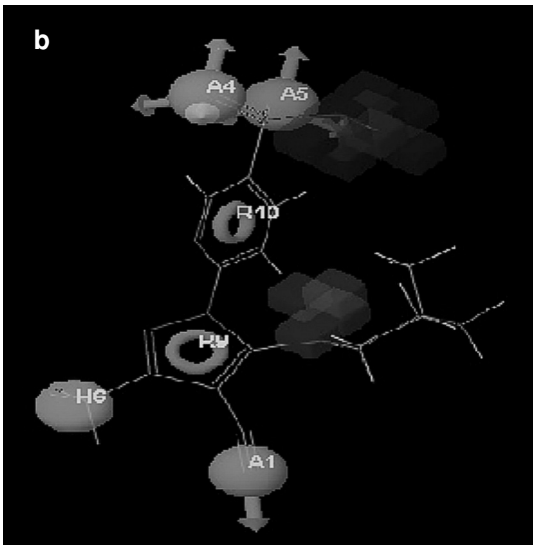


Figure. 5b. 3-D QSAR model based on least active compound **27** of the training set illustrating hydrogen bond donor feature.

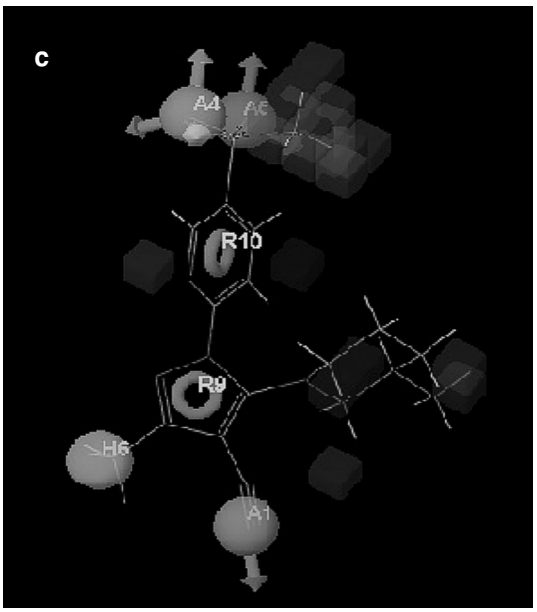


Fig. 5c. 3-D QSAR model based on more active compound **16** of the training set illustrating hydrophobic feature

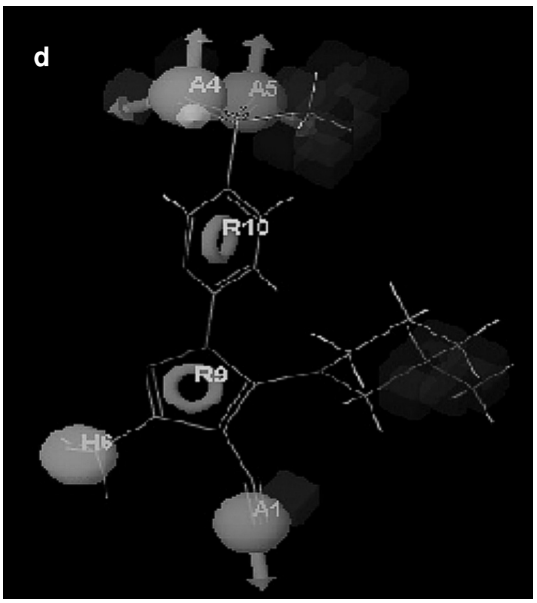


Fig. 5d. 3-D QSAR model based on more active compound **16** of the training set illustrating electron withdrawing feature.

filled with square boxes) near the methyl group indicates that substitution of any hydrophobic group at this position, decreases the activity.

The 3-D QSAR model based on electron withdrawing feature is shown in Figure 5d. The blue region (denoted by cubes filled with vertical lines) was observed near the methyl group and 5-aryl substitution of pyrazole indicating that substitution of electron withdrawing group at this position increases the activity. The red region (denoted by cubes filled with square boxes) was observed near the CN and oxygen of sulfonamide group indicating that both these groups decrease the activity. Then, replacing these groups by those groups which are not electron withdrawing, provides better results.

## CONCLUSION

3D pharmacophore hypothesis for 5-heteroatom substituted pyrazoles as COX-2 inhibitors

was studied through a ligand-based computational approach. Different pharmacophore hypothesis were developed using PHASE software, and the alignments based on these pharmacophores were used as the input for the development of 3D-QSARs. A six point pharmacophore with three hydrogen bond acceptors (A), one hydrobhobic group (H), and two aromatic rings (R) as pharmacophoric features were associated with the most significant QSAR model. This pharmacophore model could be of great interest, not only to gain insight into the structure-activity relationship of these compounds, but also to clarify the specific role of the COX-II inhibitors. The model could be used to screen compounds with various structures in search of potent COX-II inhibitory activity.

## REFERENCES


1. Rang H.P., Dale M.M., Ritter J.M., Gardner P.: Pharmacology, 3rd edn., p. 246, Churchill Livingstone, New York 1995.
2. Menozzi G., Merello L., Fossa P., Mosti L., Piana A., Mattioli F.: Farmaco 58, 795 (2003).
3. Vane J.R., Bakhle Y.S., Botting R.M.: Annu. Rev. Pharmacol. Toxicol. 38, 97 (1998).
4. Bhandari S.V., Dangre S.C., Bothara K.G., Patil A.A., Sarkate A.P., Lokwani D.K., Gore S.T. et al.: Eur. J. Med. Chem. 44, 4622 (2009).
5. Lipsky P.E.: J. Rheumatol. 26, 25 (1999).
6. Dannhardt G., Kiefer W.: Eur. J. Me. Chem. 36, 109 (2000).
7. Sengupta S.: Indian J. Pharmacol. 31, 322 (1999).
8. Hawkey C.J.: Lancet 353, 307 (1999).
9. Khannaa I.S., Weier R.M., Collins P.W. et al.: J. Med. Chem. 40, 1619 (1997).
10. Boehm J.C., Smietana J.M., Sorenson M.E. et al.: J. Med. Chem. 39, 3929 (1996).
11. Li J.J., Anderson G.D., Reitz D.B. et al.: J. Med. Chem. 38, 4570 (1995).
12. Manivannan F., Prasanna S., Chaturvedi S.C.: Indian J. Biochem. Biophys. 41, 179 (2004).
13. Tavares I.A., Bishai P.M., Bennett A., Forsch A.: Drug Res. 45, 1093 (1995).
14. Penning T.D., Talley J.J., Bertenshaw S.R., Carter J.S., Collins P.W. et al.: J. Med. Chem. 40, 1347 (1997).
15. Prasit P., Wang Z., Brideau C., Chan C.-C., Charleson S., Cromlish W., Ethier D. et al.: Bioorg. Med. Chem. Lett. 9, 1773 (1999).
16. Talley J.J., Brown D.L., Carter J.S., Graneto M.J., Koboldt C.M., Masferrer J.L., Perkins W.E. et al.: J. Med. Chem. 43, 775 (2000).
17. Sorbera L.A., Castaner R.M., Silvestre J., Castaner J.: Drugs Future 26, 346 (2001).
18. Kalgutkar A.S., Zhao Z.: Curr. Drug Targets 2, 79 (2001).
19. Pasinetti G.M.: J Neurosci. Res. 54, 1 (1998).
20. Dogne J.M., Supuran C.T., Pratico D.: J. Med. Chem. 48, 2251 (2005).
21. Mukherjee D., Nissen S.E., Topo E.J.: J. Am. Med. Assoc. 286, 954 (2001).
22. Hukki J., Laitinen P., Alberty J.E.: Pharm. Acta Helv. 43, 704 (1968).
23. Tan Y.T., Tillett D.J., Mckay I.A.: Mol. Med. Today 6, 309 (2000).
24. MacManus M.C.: Am. J. Health-Syst. Pharm. 54, 1420 (1997).
25. Dixon S.L., Smondyrev A.M., Knoll E.H., Rao S.N., Shaw D.E., Friesner R.A.: J. Comput. Aided Mol. Des. 20, 647 (2006).
26. PHASE, Version 3.0, Schrödinger, LLC, New York 2008.
27. Sakya S.M., DeMello K.M.L., Minich M.L.: Bioorg. Med. Chem. Lett. 16, 288 (2006).
28. Ligprep, Version 3.0, Schrödinger, LLC, New York 2008.
29. Chang G., Guida W., Still W.C.: J. Am. Chem. Soc. 111, 4379 (1989).
30. Kolossvary I., Guida W.C.: J. Am. Chem. Soc. 118, 5011 (1996).
31. MacroModel, Version 3.0, Schrödinger, LLC, New York 2008.
32. SMART – Language for Describing Molecular Patterns, Daylight Chemical Information System, Inc., Aliso Viejo, CA.
33. Pasha F.A., Muddassar M., Jung H., Yang B.S., Lee C.: Bull. Korean Chem. Soc. 29, 647 (2008).


*Received: 30. 03. 2011*